

Warming leads to both earlier and later snowmelt floods over the past 70 years

Received: 28 November 2024

Accepted: 3 April 2025

Published online: 17 April 2025



Yuhan Guo^{1,2}, Yuting Yang^{1,2}✉, Dawen Yang^{1,2}✉, Lu Zhang³,
Hongxing Zheng⁴, Jinghua Xiong^{1,2}, Fangzheng Ruan^{1,2}, Juntai Han^{1,2} &
Ziwei Liu⁵

Climate warming reduces snow cover in cold regions, altering snowmelt flood regimes with significant hydrological and ecological consequences. Existing evidence indicates that as climate warms, snowmelt tends to begin earlier in the season, leading to earlier snowmelt floods. Here we show that the timing of snowmelt floods can be either advanced or delayed under warming. Using streamflow observations from 1950–2020 and an event-based analysis that distinguishes flood-generating mechanisms across 2339 Northern Hemisphere, snow-affected catchments, we show that the earlier snowmelt effect can be substantially offset or even reversed by a decelerated snowmelt rate under warming. This results in delayed snowmelt floods in approximately 30% of the catchments, contributing to an overall minor shift on a hemispheric scale (-0.87 ± 2.4 days per decade). Our findings challenge the prevailing “warming leads to earlier snowmelt floods” paradigm, revealing a more complex pattern of changes in snowmelt flood in a warming world.

Flooding is among the most devastating natural hazards, with annual global economic losses exceeding US\$100 billion^{1,2}. In recent decades, flood-related damage has intensified in many regions of the globe, a trend expected to worsen due to the increasing frequency of extreme weather events driven by climate change^{3–5}. On a global scale, the frequency and intensity of extreme rainfall events have risen in response to warming-induced increases in atmospheric moisture capacity, leading to more frequent and severe flooding in many areas^{6,7}. Unlike rainfall-induced floods, snowmelt floods are more complex and exhibit greater sensitivity to rising temperatures^{8–12}. In snow-affected regions, warming is reducing the proportion of precipitation falling as snow and advancing snowmelt timing^{13–15}. This alteration in snow dynamics is anticipated to lead to earlier snowmelt floods, with profound implications for flood forecasting, mitigation strategies, and the health of aquatic and riparian ecosystems^{16,17}.

Several studies have reported shifts toward earlier snowmelt flood timing across snow-affected catchments (Supplementary Table 1).

However, these studies have primarily focused on local or regional scales, with considerable variability in estimates of snowmelt flood timing sensitivity to warming and lacking a comprehensive global synthesis^{8,18–24}. More critically, previous studies often utilized methods such as annual maximum peak flow or peaks-over-threshold to identify flood events, categorizing snowmelt floods based on catchment location or the mean timing of flood occurrences^{8,21–23}. These approaches assume that all annual maximum floods in snow-affected catchments, or those occurring during winter or spring, are driven by snowmelt. However, this assumption is not always valid, as floods during these periods in snow-affected regions may also be triggered by other mechanisms, such as storms, prolonged rainfall, or rain on snow^{7,25,26}. This methodological limitation introduces significant uncertainty into our understanding of changes in snowmelt flood regimes, which is critical for enhancing flood preparedness and management strategies in snow-affected regions and beyond. Despite the importance of this issue, direct observational evidence on changes in snowmelt flood timing remains limited.

¹State Key Laboratory of Hydrosience and Engineering, Tsinghua University, Beijing, China. ²Department of Hydraulic Engineering, Tsinghua University, Beijing, China. ³State Key Laboratory of Water Resources and Hydropower Engineering Science, Wuhan University, Wuhan, China. ⁴CSIRO Environment, Black Mountain, Canberra, Australia. ⁵Department of Civil and Environmental Engineering, College of Design and Engineering, National University of Singapore, Singapore, Singapore. ✉e-mail: yuting_yang@tsinghua.edu.cn; yangdw@tsinghua.edu.cn

To address these limitations and provide a more direct observational assessment of shifts in snowmelt flood timing under historical climate change, here we applied an event-based approach to 2339 snow-affected, unimpaired catchments across the Northern Hemisphere from 1950 to 2020. A total of 243,073 flood events were identified, and a classification algorithm was used to categorize these events into distinct flood types^{7,27} (also see *Methods*). The annual maximum snowmelt-induced flood events were then analyzed. Our findings reveal a complex evolution of snowmelt flood timing over the past 70 years. While a general trend toward earlier snowmelt floods was observed on a hemispheric scale, partially corroborating previous

studies, we also identified numerous cases of delayed snowmelt floods primarily associated with slower snowmelt rates.

Results

To investigate shifts in snowmelt flood timing under warming, we first examined trends in annual mean temperature, the maximum snow water equivalent (SWE_{max}) and the timing of annual maximum snowmelt flood (t_{sf}) across 2339 catchments from 1950 to 2020 (Fig. 1). Our results indicate that 2278 catchments (approximately 97%) experienced an increase in annual mean temperature over the past seven decades, with an average rise of 0.22 °C per decade (Fig. 1a,b). This

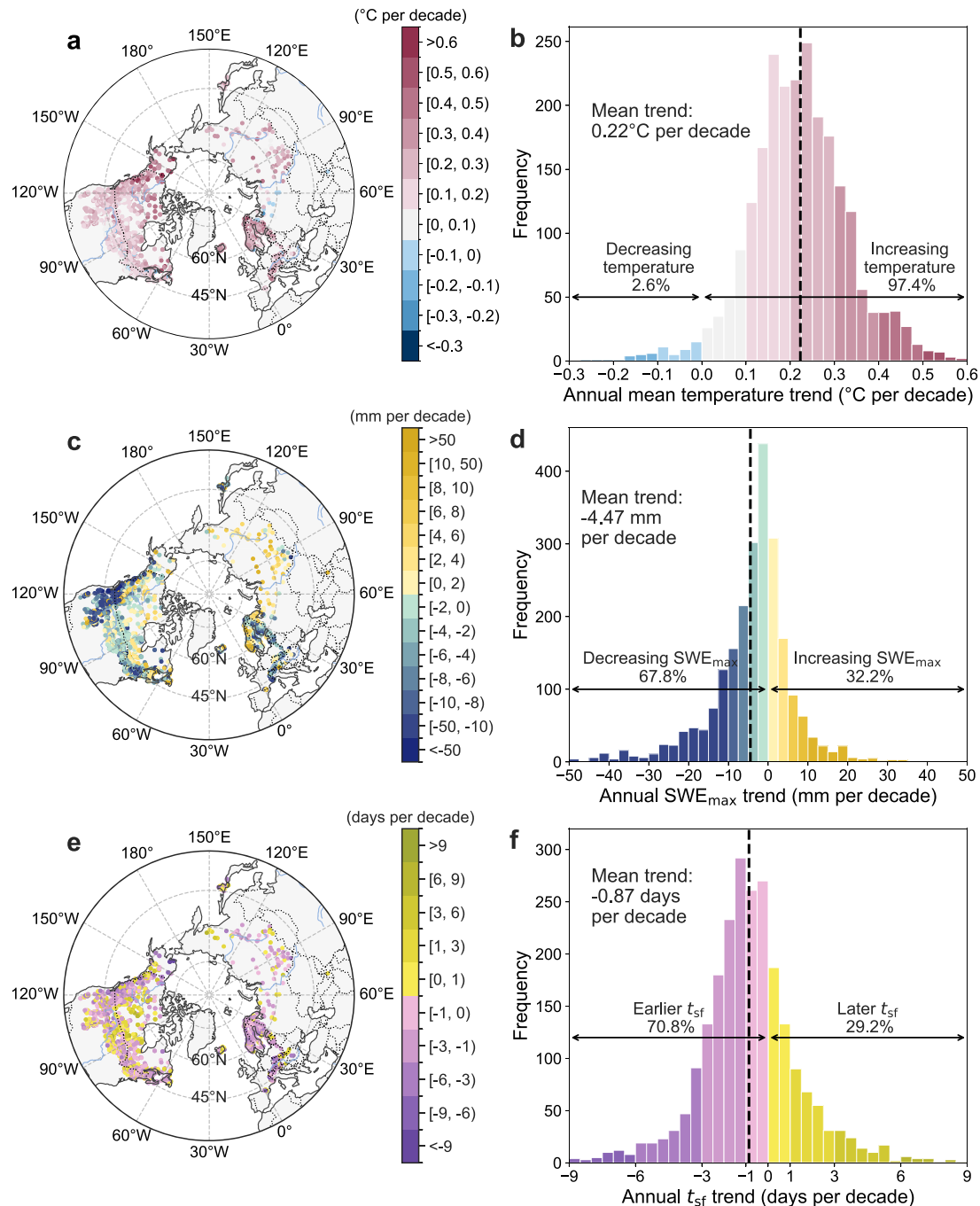


Fig. 1 | Trends in temperature, maximum snow water equivalent, and snowmelt flood timing across 2339 catchments over 1950–2020. a | Spatial distribution of trends in annual mean air temperature. **b** | Histogram of trends in annual mean air temperature. **c** | Spatial distribution of trends in annual maximum snow water

equivalent (SWE_{max}). **d** | Histogram of trends in SWE_{max} . **e** | Spatial distribution of trends in annual snowmelt flood timing (t_{sf}). **f** | Histogram of trends in annual t_{sf} . In (**b**, **d**, and **f**), the vertical dashed lines represent the mean trends. Source data are provided as a Source Data file.

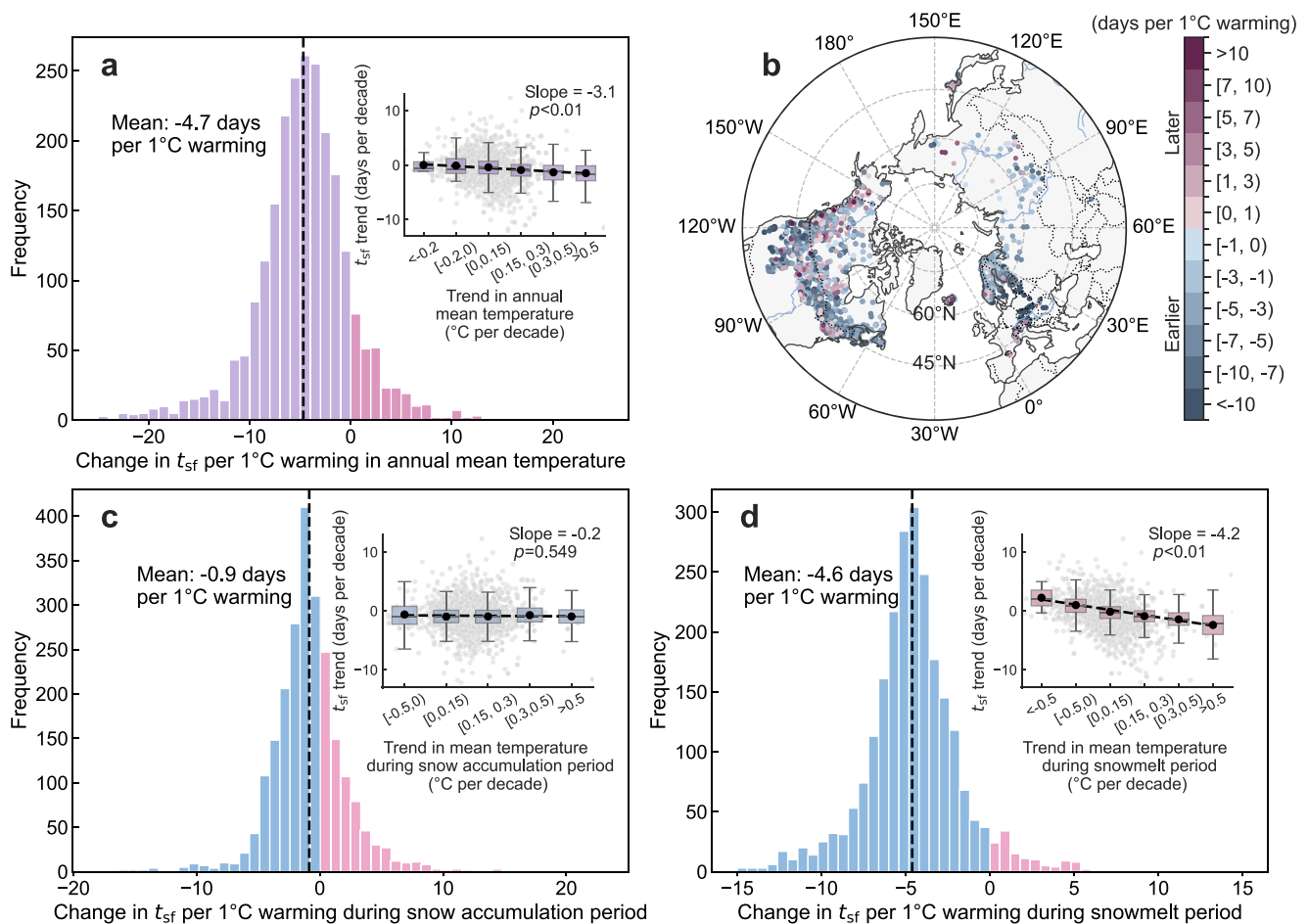


Fig. 2 | Sensitivity of snowmelt flood timing to warming. **a** | Histogram illustrating the sensitivity of snowmelt flood timing (t_{sf}) to warming in annual mean air temperature across 2339 catchments. **b** | Spatial distribution of t_{sf} sensitivity to warming in annual mean air temperature across 2339 catchments. **c** | Histogram of t_{sf} sensitivity to warming during snow accumulation period across 2339 catchments. **d** | Histogram of t_{sf} sensitivity to warming during snowmelt period across 2339 catchments. In **(a, c, and d)**, the vertical dashed lines represent the mean

sensitivities. The box plots within **(a, c, and d)** show the relationship between trends in t_{sf} and trends in temperature across these catchments. Whiskers represent the 1st and 99th percentile, with the top and bottom of each box indicating the 25th and 75th percentiles, respectively. The horizontal line inside each box represents the median, while black dots indicate the mean. The dashed lines indicate the best linear fit across all individual catchments. Source data is provided as a Source Data file.

warming trend is particularly pronounced in high-latitude and high-elevation catchments, which typically have lower mean annual temperatures, compared to those at lower latitudes and elevations (Supplementary Fig. 1). In terms of SWE_{max} , about 68% of catchments exhibited a decline, with an average reduction of 4.47 mm per decade (Fig. 1c,d). The most significant declines in SWE_{max} were observed along the Rocky Mountains, eastern Europe, and the Alps, while slight increases occurred in the northern Pacific Mountain Ranges, Kjolen Mountains, and parts of Siberia. Regarding t_{sf} , 1654 catchments (-70.8%) experienced earlier snowmelt flood events, with the majority showing advancements of less than 3 days per decade (Fig. 1e,f). Notably, only 56 catchments exhibited advancements longer than 6 days per decade, scattered across both North America and Europe, with evident hotspots in the northern Europe and the Alps. Conversely, 685 catchments demonstrated delayed snowmelt flood timing, distributed widely across the Northern Hemisphere without distinct regional patterns. On average, t_{sf} advanced by 0.87 ± 2.4 (mean \pm 1 s.d.) days per decade over the past 70 years, shifting from mid-May in the 1950s to early May in the 2010s (Supplementary Fig. 2).

We next analyzed the sensitivity of t_{sf} to warming (i.e., the slope of the relationship between temperature and t_{sf}) for each catchment (Fig. 2). On average, a 1 °C increase in annual mean temperature is associated with an advancement of t_{sf} by 4.7 ± 5.0 days (mean \pm 1 s.d.).

This relationship is further supported by a significant negative correlation between the trend in t_{sf} and the trend in annual mean temperature across 2339 catchments ($p < 0.01$, t -test; Fig. 2a). Moreover, the sensitivity of t_{sf} to warming generally increases with mean annual temperature, with warmer catchments generally exhibiting a greater negative sensitivity compared to colder ones (Fig. 2b and Supplementary Fig. 3). Specifically, in catchments with mean annual temperatures below -5 °C, t_{sf} advances by approximately 1.7 days for each 1 °C increase in annual mean temperature, whereas relatively warmer catchments (mean annual temperature > 5 °C) demonstrate a sensitivity of 5.8 days per 1 °C warming. Beyond the annual mean temperature, we also evaluated the t_{sf} sensitivity using mean temperatures during the snow accumulation and snowmelt periods (Fig. 2c,d). Our analysis indicates that the trend in t_{sf} is only weakly correlated with the trend in temperature during the snow accumulation period ($p = 0.549$, t -test) but strongly correlated with temperature trends during the snowmelt period ($p < 0.01$, t -test), suggesting that warming during the snow melting period predominantly influences the timing of snowmelt floods.

To reveal causes of shifts in snowmelt flood timing, we first performed correlation analyses between t_{sf} and a range of climate and snow dynamics attributes to identify factors affecting t_{sf} . This analysis highlighted five key attributes (Fig. 3a), three of which are associated

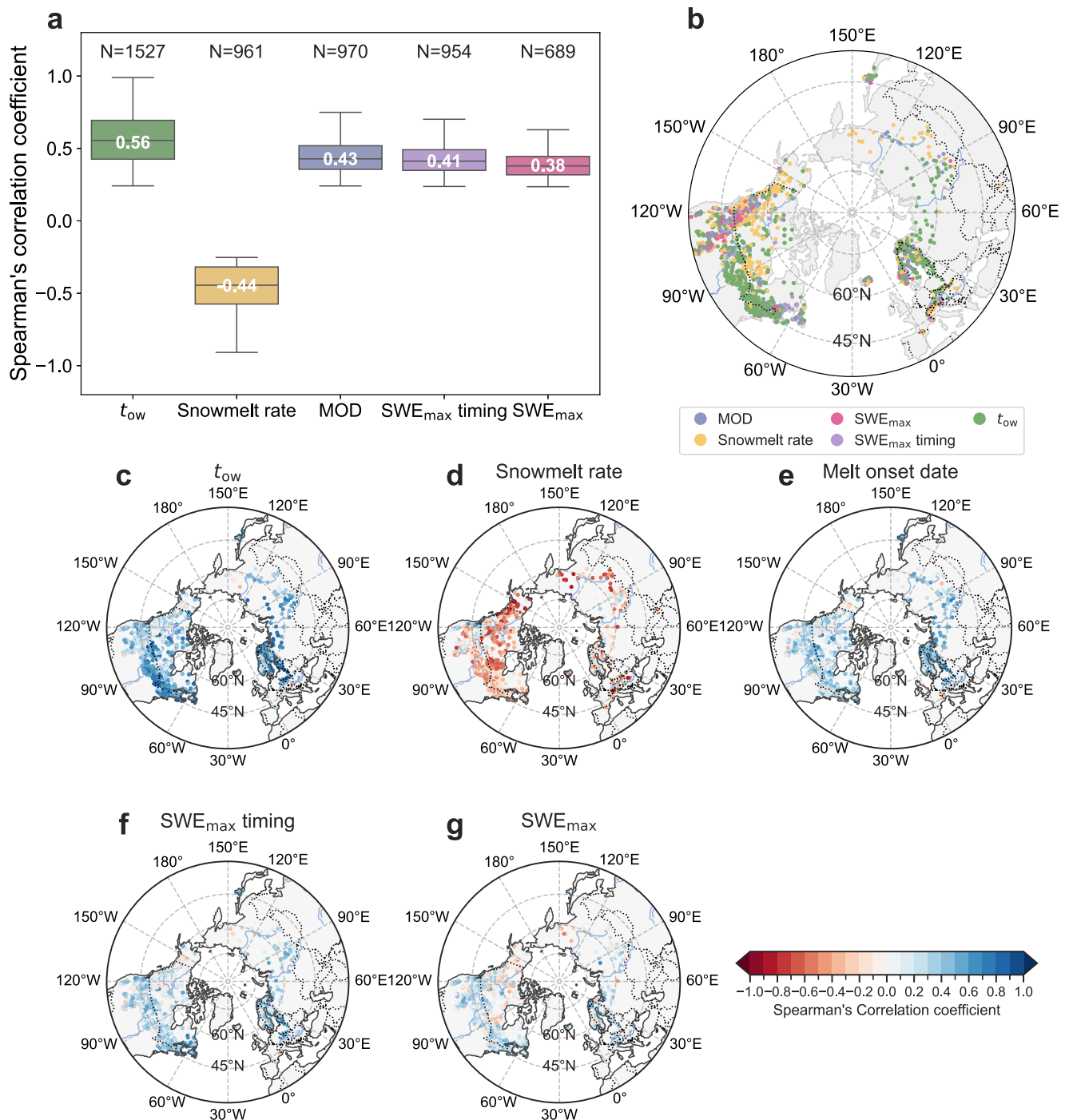


Fig. 3 | Factors affecting snowmelt flood timing. a | Boxplot of Spearman's correlation coefficient between snowmelt flood timing (t_{sf}) and five key variables: onset of seasonal warming (t_{ow}), snowmelt rate, maximum snow water equivalent (SWE_{max}) timing, melt onset date, and SWE_{max} . The number above each box indicates the number of catchments where the correlation is statistically significant ($p < 0.05$, t -test), and the number within each box indicates the median value.

b | Spatial distribution of dominant factors controlling t_{sf} , revealed by comparing the correlation strengths between t_{sf} and the five key variables. **c–g** | Spatial distribution of Spearman's correlation coefficient between t_{sf} and each of the five variables: **(c)**, t_{ow} , **(d)**, snowmelt rate, **(e)**, SWE_{max} timing, **(f)**, melt onset date, and **(g)**, SWE_{max} , respectively. Source data is provided as a Source Data file.

with the timing of snow or temperature events. These include the onset of seasonal warming (t_{ow}), the timing of maximum snow water equivalent (SWE_{max}), and the onset of snowmelt, all of which have advanced in most catchments over the past seven decades (Supplementary Fig. 4). In principle, t_{sf} can be directly influenced by the timing of SWE_{max} or the melt onset date (MOD). Our results confirm that earlier SWE_{max} or MOD typically results in earlier snowmelt floods (Fig. 3a). However, compared to SWE_{max} and MOD, t_{ow} exhibits the

strongest correlation with t_{sf} , suggesting that the timing of seasonal temperature rise is the predominant factor controlling snowmelt flood timing on a hemispheric scale (Fig. 3a). In addition to the three timing-related attributes, the magnitude of SWE_{max} and the rate of snowmelt are also reasonably correlated with t_{sf} , with a lower SWE_{max} or a faster snowmelt rate generally associated with an earlier t_{sf} (Fig. 3a).

Locally, the correlation between t_{ow} and t_{sf} is strongest in 1128 catchments, spanning mid-latitude North America, Europe, and central

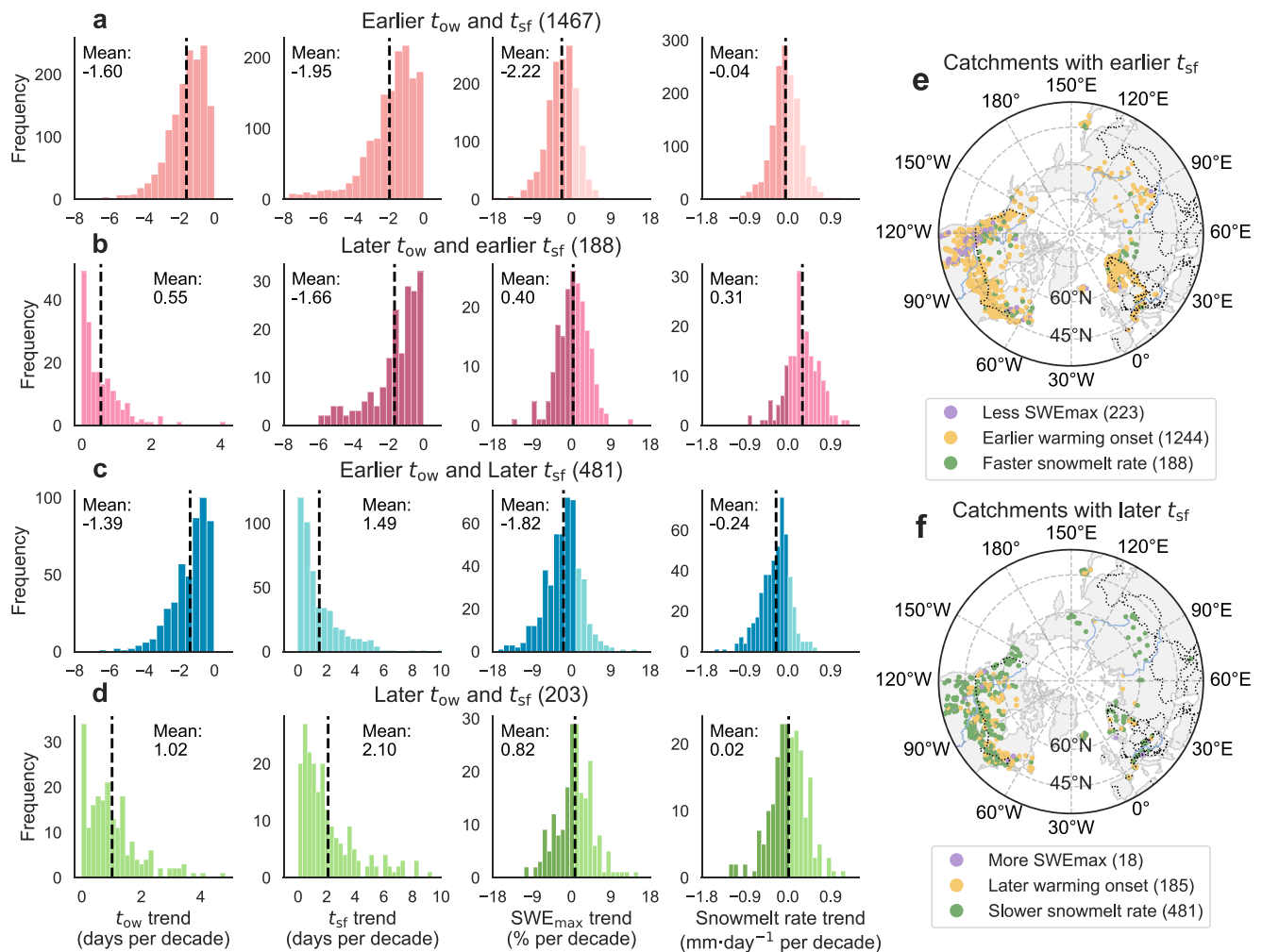


Fig. 4 | Attribution of changes in snowmelt flood timing. a–d | Histograms of trends in onset of seasonal warming (t_{ow}), snowmelt flood timing (t_{sf}), the maximum snow water equivalent (SWE_{max}) and snowmelt rate in catchments with (a), advanced t_{sf} and t_{ow} , (b) advanced t_{sf} and delayed t_{ow} , (c) delayed t_{sf} and advanced t_{ow} , and (d), delayed t_{sf} and t_{ow} . The vertical dashed lines represent the mean trends.

e | Spatial distribution of dominant factors contributing to earlier T_{sf} . **f** | Spatial distribution of dominant factors contributing to later T_{sf} . The number in parentheses indicates the number of catchments. Source data is provided as a Source Data file.

Siberia (Fig. 3b,c), reinforcing the pivotal role of t_{ow} in controlling t_{sf} across these regions. Following t_{ow} , the snowmelt rate exerts the dominant influence on t_{sf} in 564 catchments, which are primarily in colder regions such as high-latitude North America, the Rocky Mountains, the Alps, and Russia's Far East (Fig. 3b,d). For the remaining factors, MOD, SWE_{max} timing, and SWE_{max} magnitude are the primary controls on T_{sf} in 242, 187, and 218 catchments, respectively (Fig. 3b,e–g).

The above results indicate that t_{ow} generally outweighed other factors in controlling t_{sf} . However, among the 2339 catchments analyzed, 83.3% experienced an earlier t_{ow} (Supplementary Fig. 4), which is notably higher than the 70.8% of catchments showing earlier t_{sf} (Fig. 1f). This suggests that t_{ow} alone cannot fully explain changes in t_{sf} . To gain deeper insights into t_{sf} changes, here we classified the catchments into four groups based on distinct trends in t_{ow} and t_{sf} : (1) advanced t_{sf} and t_{ow} , (2) advanced t_{sf} and delayed t_{ow} , (3) delayed t_{sf} and advanced t_{ow} , and (4) delayed t_{sf} and t_{ow} . In addition to t_{ow} and t_{sf} , we also examined changes in SWE_{max} and snowmelt rate for each group of catchments. The timing of SWE_{max} and MOD were excluded from further analysis as they closely mirror t_{ow} (all provide timing information) and exhibit a strong linear relationship with it (Supplementary Fig. 5).

We find that in group-1 catchments where both t_{sf} and t_{ow} advanced over the past 70 years, SWE_{max} shows a clear decreasing trend, while changes in the snowmelt rate are minimal (Fig. 4a). This suggests that the earlier t_{sf} in group-1 catchments is driven by either earlier t_{ow} or declining SWE_{max}, with the latter effect being particularly dominant in the Rocky Mountain ranges (Fig. 4e). In group-2 catchments, where t_{sf} advanced but t_{ow} was delayed, SWE_{max} remains relatively unchanged, while the snowmelt rate increased, indicating that the earlier t_{sf} is primarily driven by the accelerated snowmelt in these catchments (Fig. 4b). However, catchments in this category are relatively scarce, predominantly scattered across high-latitude regions of North America and central Euro-Asia (Fig. 4e). Group-3 catchments, which exhibited delayed t_{sf} alongside advanced t_{ow} and decreased SWE_{max}, experienced a dramatic decrease in snowmelt rate. This reduction in snowmelt rate outweighed the effects of t_{ow} and SWE_{max}, leading to the delayed t_{sf} in these catchments (Fig. 4c). In group-4 catchments, snowmelt rate remained essentially unchanged, and SWE_{max} slightly increased. The delay in t_{sf} in most of these catchments was primarily driven by the later t_{ow} , with the increased SWE_{max} contributing to the delay in t_{sf} in a limited number of catchments scattered across the central and along east coast of North America (Fig. 4d,f).

Discussion

As one of the most rapidly changing components of the Earth's system, declining snow under warming has profound impacts on terrestrial hydrological processes, including streamflow volume and seasonal patterns^{28–30}, as well as extreme hydrological events^{31,32}. While existing evidence suggests that declining snow is likely to reduce the magnitude of snowmelt-driven floods^{7,15}, direct assessments of how snowmelt flood timing responds to warming remain limited. Using long-term streamflow observations and distinguishing flood generation mechanisms, we provide the first hemispheric-scale observational assessment of shifts in the timing of snowmelt floods over the past 70 years.

Our results reveal a complex pattern of change in snowmelt flood timing under warming across Northern Hemisphere catchments. On a hemispheric scale, we find that the average t_{sf} advanced by 0.87 days per decade from 1950 to 2020, corresponding to a sensitivity of approximately 4.7 days earlier for every 1 °C of warming (Figs. 1e,f, 2a). While this overall advancement in t_{sf} aligns with previous regional findings^{8,18–23}, significant variability exists among individual catchments, with nearly 30% of them demonstrating delayed t_{sf} (Fig. 1e,f). This results in a standard deviation of t_{sf} trends that is 2.7 times greater than the mean trend. Furthermore, when applying a threshold of $< \pm 1$ day per decade to indicate no change²⁴, the derived mean t_{sf} trend is minimal, suggesting a lack of evidence for an earlier t_{sf} at the hemispheric scale. This conclusion somewhat contradicts previous findings that reported a predominant shift towards earlier t_{sf} in various regions^{8,18–24}. This discrepancy can be partly attributed to the larger scale of the current analysis, but a more critical issue arises from prior studies that often categorize snowmelt floods based on catchment location or average flood timing^{8,21–23}, potentially introducing significant uncertainties in identifying snowmelt floods. For instance, in historically snow-dominated regions, reduced winter snowfall due to rising temperatures or changing precipitation patterns may have shifted the flood regime from spring snowmelt floods to more frequent rainfall-induced floods in winter^{11,33}. Failure to distinguish between different flood generation mechanisms could misclassify these rainfall-induced winter floods as snowmelt floods, leading to erroneous conclusions regarding t_{sf} changes under such conditions.

The onset of seasonal warming and the rate of snowmelt have been identified as the two key drivers of shifts in t_{sf} (Fig. 3). The former predominantly influences catchments with advanced t_{sf} , while the latter is more significant in catchments experiencing delayed t_{sf} (Fig. 4e,f). Theoretically, the onset of seasonal warming indicates the timing of snowmelt and the rate of snowmelt depicts how fast snow melts, and an earlier warming onset and faster snowmelt should lead to an earlier t_{sf} . Existing evidence overwhelmingly points to earlier snowmelt under warming conditions^{15,16,34–36}, however, it also reveals a general trend toward decelerated snowmelt due to a contraction of the melt season into periods with lower energy availability following the advancement of snowmelt^{37–39}. Our results confirm these previous findings, with most catchments exhibiting an earlier t_{ow} and a slower rate of snowmelt (Supplementary Fig. 4). These two changes in snow dynamics, while both driven by warming, can exert opposing effects on t_{sf} (Fig. 3a–d). Previous studies have primarily attributed the earlier t_{sf} to earlier snowmelt, often overlooking the impact of changes in snowmelt rates^{10,11,14}. However, our findings demonstrate a significant negative relationship between snowmelt rate and t_{sf} , suggesting that the reduced snowmelt rate may slowed or even reversed the previously reported trend of advancing t_{sf} under warming. This phenomenon is likely driven by two mechanisms. First, under slower melting conditions, a longer period is required for snowmelt water to accumulate to levels sufficient to trigger a flood event. Second, slower snowmelt may result in smaller discharge peaks, which might not consistently exceed the threshold necessary to qualify as a flood.

Consequently, the negative correlation observed between t_{sf} and snowmelt rate may, in part, reflect a reduction in the frequency of snowmelt floods (Supplementary Figs. 6, 7).

In addition to t_{ow} and snowmelt rate, we also observe a positive relationship between t_{sf} and the magnitude of SWE_{max} . Declines in SWE_{max} indicate reduced snow cover, which lowers surface albedo and consequently increases absorbed radiative energy at the ground surface^{9,28}. This enhanced energy availability promotes earlier snowmelt timing, leading to earlier t_{sf} . This effect is particularly pronounced along the Rocky Mountain ranges, where the most substantial declines in SWE_{max} have been observed over the past 70 years (Figs. 1c, 3b and 4e).

An intriguing question arises: since t_{ow} indicates the timing of snowmelt, why does the determined MOD show a weaker correlation with t_{sf} compared to the correlation between t_{ow} and t_{sf} ? Indeed, t_{ow} and the MOD are closely linked (Supplementary Fig. 5). However, conventional approaches to determining MOD based on SWE time series may involve substantial uncertainties in catchments or years with multiple SWE peaks, complicating the distinction between snow accumulation and snowmelt periods (see an example in Supplementary Fig. 8). In contrast, temperature time series are typically much simpler, exhibiting clear cooling and warming periods, thereby facilitating a more straightforward determination of t_{ow} . More fundamentally, changes in SWE are influenced not only by temperature but also by precipitation, which can exhibit greater day-to-day variability than temperature.

The contrasting effects of earlier t_{ow} , declining SWE_{max} , and slower snowmelt collectively contribute to an overall minor yet locally variable evolution of t_{sf} across the Northern Hemisphere. Despite these complexities, several notable patterns emerge. Consistent with previous findings⁴⁰, larger warming trends are generally found in colder catchments (Supplementary Fig. 1). Furthermore, as mean annual temperature rises, we find more advanced t_{ow} , greater reductions in SWE_{max} , and faster declines in snowmelt rates, which together result in insignificant changes in t_{sf} trends along the temperature gradient (Supplementary Fig. 9). This lack of significant change in t_{sf} trends with temperature, coupled with smaller warming trends in relatively warmer catchments, accounts for the observed higher sensitivity of t_{sf} to warming in catchments with a higher mean annual temperature (Fig. 2 and Supplementary Fig. 3). Nevertheless, it is important to note that this increasing sensitivity of t_{sf} to warming with mean annual temperature holds only for catchments with mean annual temperatures below approximately 6 °C. For catchments with mean annual temperatures exceeding ~6 °C, the warming trends are relatively weaker, leading to smaller reductions in SWE_{max} and consequently less pronounced changes in t_{sf} (Supplementary Fig. 9). As a result, the sensitivity of t_{sf} to warming is also relatively smaller in these warmer catchments (Supplementary Fig. 3).

Our findings of both advancing and delaying t_{sf} have important hydrological and ecological implications. From a hydrological perspective, the earlier t_{sf} observed in most northern catchments suggests a seasonal shift in water resources toward the earlier in the year. This shift may reduce water availability and potentially increase the frequency and severity of droughts during summer and autumn in catchments that are heavily dependent on snowmelt for streamflow^{15,36}. Conversely, in catchments experiencing a delay in t_{sf} , while the risk of spring floods may be mitigated, the postponed snowmelt floods—when combined with heavy rainfall—could substantially elevate the risk of summer flooding⁴¹. From an ecological standpoint, changes in t_{sf} may disrupt the reproductive processes and habitats of both in-river and riparian species, affecting fish migration, waterbird breeding, and vegetation seeding⁴². Nevertheless, snowmelt floods are a complex phenomenon involving multiple opposing responses of snow dynamics to warming, leading to a more intricate pattern of t_{sf} changes across northern catchments than previously

understood. Despite that, elucidating the mechanisms driving these complex t_{sf} changes could enhance our modeling of snowmelt floods, thereby improving our ability to predict future changes under ongoing warming.

Methods

Datasets

Daily streamflow (Q) observations from 1950 to 2020 were collected for 2339 catchments across the Northern Hemisphere, sourced from 8 databases: (i) the Global Runoff Data Centre (<https://portal.grdc.bafg.de>), (ii) the USGS National Water Information System (https://waterdata.usgs.gov/nwis/dv?referred_module=sw&search_criteria=huc2_cd&search_criteria=site_tp_cd&submitted_form=introduction), (iii) the Water Survey of Canada Hydrometric Data (https://wateroffice.ec.gc.ca/mainmenu/historical_data_index_e.html), (iv) Eaufrance service (<https://hubeau.eaufrance.fr/page/a-propos>), (v) Japanese Water Information System (www1.river.go.jp/); (vi) Center for Studies and Experimentation of Public Works (<https://ceh.cedex.es/anuarioaforos/default.asp>), (vii) New Russian Daily Discharge Data from NSF-funded UCLA/UNH project (<https://www.r-arcticnet.sr.unh.edu/v4.0/AllData/index.html>), and (viii) Collaborative UAF/UNH Research: Study of Dam/Reservoir-induced Hydrologic Changes in Siberian Regions: Regional Analysis to Pan-Arctic Synthesis (<https://www.r-arcticnet.sr.unh.edu/ObservedAndNaturalizedDischarge-Website/>). The selected catchments each have continuous daily Q records spanning at least 30 years, with catchment sizes ranging from 100 to 100,000 km². A lower size threshold of 100 km² ensures that the catchments encompass at least one grid cell of meteorological forcing data (approximately 9 × 9 km² spatial resolution), while the upper threshold of 100,000 km² was applied to avoid catchments with extremely long residence times. To focus on snowmelt flood, all catchments have a mean annual snowfall fraction—defined as the proportion of precipitation that falls as snow—greater than 10%, and a snow cover percentage exceeding 10%. Additionally, to minimize anthropogenic influences, these catchments were selected based on the following criteria: irrigation areas less than 5% (Global Map of Irrigation Areas-GMIA⁴³), urban area less than 5% (MODIS Land Cover Dataset⁴⁴), and reservoir capacity smaller than 5% of the mean annual Q (Global Reservoir and Dam Database⁴⁵). Consequently, the 2339 catchments exhibited mean irrigation and urban areas comprising 0.18% and 0.13% of the mean catchment area, respectively, with mean reservoir capacity being 0.18% of the mean annual Q . A consistent water year, defined as October 1 to September 30 of the following calendar year, was applied across all catchments, resulting in the exclusion of those located in the Southern Hemisphere.

Hourly precipitation, near-surface air temperature, snowfall, snowmelt, and snow water equivalent (SWE) data from 1950 to 2020 were obtained at 0.1° spatial resolution from the fifth generation of the European Reanalysis (ERA5-Land) dataset⁴⁶. These gridded data were upscaled to daily values using averages or accumulations for each grid, and subsequently spatially aggregated for each catchment. The ERA5-Land dataset, characterized by its long temporal coverage and high spatial resolution, has been rigorously evaluated against observations, confirming its accuracy and suitability for long-term hydrological studies^{46,47}. To assess the potential impact of uncertainty in the ERA5-Land SWE data on our results, additional uncertainty analyses were conducted. These included two approaches: (1) sensitivity analysis, and (2) comparison with alternative global SWE datasets, i.e., the original ERA5⁴⁸ and GlobSnow⁴⁹. The results of these analyses indicated that the uncertainty in the ERA5-Land SWE data had only a minor effect on our conclusions regarding the timing shifts of snowmelt floods (Supplementary Figs. 10–15).

Flood type classification

The identification of snowmelt-induced flood events involves two key steps: (i) flood event identification using a peaks-over-threshold

approach⁵⁰, and (ii) flood type classification using the method outlined in ref. 7.

Specifically, flood identification follows a structured process: (i) baseflow separation, (ii) identification of flood start and end points as well as peak values, and (iii) merging multi-peak flood events and re-identifying start and end points. Baseflow separation was performed using the optimal baseflow method for each catchment, as outlined ref. 51. (<https://github.com/xiejx5/baseflow/tree/master>). The flood start and end points, along with peak values, were initially identified by determining the magnitude of daily Q corresponding to the 90th percentile of the daily Q series for each catchment, which served as the threshold for flood peak identification. Using a higher threshold (i.e., the 95th percentile of the daily Q series) yielded similar results (Supplementary Figs. 16, 17). Any local peak exceeding this threshold was considered a flood event. For catchments with a low baseflow coefficient (<0.5), the start and end of a flood were identified where total runoff equals baseflow. In catchments with a high baseflow coefficient (>0.5), stable valley points—defined as runoff values that remain constant (i.e., not changing by more than 0.01 mm over a week)—were used to mark the flood's start and end points. Multi-peak flood events with overlapping valley points were merged based on two conditions. First, if both the start and end valley points were duplicated, the floods were directly merged into a single event. Second, if the end valley of one flood overlapped or closely coincided with the start valley of another, the peak value ratio between the two floods was evaluated. If the ratio exceeded a threshold of 2.5, the floods were merged⁵². Following the merging process, the start and end points of these combined flood events were re-identified.

Flood events were categorized into three main types: (i) rainfall-induced floods, (ii) rain-on-snow floods, and (iii) snowmelt floods. In this study, we employed a process-based approach for flood classification, which has been widely adopted in flood classifications globally^{7,53}. Specifically, the classification method relies on several indicators, including the intensity of snowmelt and rainfall during both the response period and the flood rising period. Flood events characterized by significant snowmelt intensity with minimal or no rainfall are classified as snowmelt floods. Conversely, events with substantial rainfall and negligible snowmelt are categorized as rainfall-induced floods. When high-intensity rainfall coincides with minor snowmelt, the flood is classified as a rain-on-snow flood. For this analysis, we utilized flood classification indicators provided by ref. 7, where the threshold values are determined using decision tree analysis, statistical clustering algorithms, and the SCE-UA global optimization method⁵⁴. Sensitivity analyses of the classification thresholds and uncertainty analyses of the classification results were conducted to enhance the reliability of the flood categorization⁷. A total of 243,073 flood events from 2339 snow-affected catchments were classified into the three flood types, with 109,919 events categorized as snowmelt-induced floods. The spatial distributions of the proportions of the three flood types are presented in Supplementary Fig. 18.

Among the identified 109,919 snowmelt flood events, our analysis focuses on the annual maximum snowmelt flood events for each catchment. These events exhibit a high degree of overlap with the annual first snowmelt floods, with approximately 90% of the annual maximum snowmelt floods coinciding with the first snowmelt flood of each year, on average, across all 2339 catchments (Supplementary Fig. 19). Additionally, about 80% of the annual maximum snowmelt floods correspond to the annual maximum flood events (Supplementary Fig. 20). The mean ratio of the magnitude of the annual maximum snowmelt floods to that of the annual maximum floods is approximately 0.94 (Supplementary Fig. 21), indicating that snowmelt floods are the predominant type of major floods in these snow-affected catchments.

Determination of key variables

Several key variables were utilized in our analyses, including snowmelt flood timing, maximum snow water equivalent (SWE_{max}), the timing of SWE_{max} , the onset of seasonal warming, snowmelt rate, and the melt onset date. Supplementary Fig. 22 provides an example illustrating the definitions of these key variables.

Specifically, snowmelt flood timing (t_{sf}) refers to the date of the peak of the annual maximum snowmelt flood event. SWE_{max} is defined as the maximum daily SWE observed each water year, while the timing of SWE_{max} is the date when this maximum occurs. It is important to note that SWE_{max} can persist for several days without further snow accumulation until snowmelt begins⁵⁵. In such cases, the timing of SWE_{max} is defined as the first day when SWE_{max} is recorded. The onset of seasonal warming (t_{ow}) is determined as the date when cumulative temperature reaches its minimum within each water year. Snowmelt rate refers to the average rate of snowmelt during the period between t_{ow} and t_{sf} . The melt onset date (MOD) was determined following the method of Clow¹⁶, where MOD is identified as the start of the first 5-day period during which SWE decreases by more than 2.5 cm.

Data availability

The hourly ERA5-Land data are available from the Copernicus Climate Change Service (C3S) Climate Data Store at <https://cds.climate.copernicus.eu/cdsapp#!/dataset/reanalysis-era5-land?tab=overview>. Streamflow data are available from 11 sources described in the Methods and metadata for the 2339 catchments used in the analyses are available at <https://doi.org/10.5281/zenodo.13892758>. Source data for generating Figs. 1–4 are provided with this paper. Source data are provided with this paper.

Code availability

The code for flood identification and classification is available at Zenodo⁵⁶.

References

- Hirabayashi, Y. et al. Global flood risk under climate change. *Nat. Clim. Change* **3**, 816–821 (2013).
- (UNISDR), U. N. O. f. D. R. R. Making development sustainable: the future of disaster risk management. Global assessment report on disaster risk reduction. (2015).
- Jongman, B., Ward, P. J. & Aerts, J. C. Global exposure to river and coastal flooding: Long term trends and changes. *Glob. Environ. Change* **22**, 823–835 (2012).
- Xiong, J. & Yang, Y. Climate change and hydrological extremes. *Curr. Clim. Change Rep.* **11**, 1 (2025).
- Winsemius, H. C. et al. Global drivers of future river flood risk. *Nat. Clim. Change* **6**, 381–385 (2016).
- Yin, J. et al. Large increase in global storm runoff extremes driven by climate and anthropogenic changes. *Nat. Commun.* **9**, 4389 (2018).
- Zhang, S. et al. Reconciling disagreement on global river flood changes in a warming climate. *Nat. Clim. Change* **12**, 1160–1167 (2022).
- Burn, D. H. & Whitfield, P. H. Changes in floods and flood regimes in Canada. *Can. Water Resour. J.* **41**, 139–150 (2016).
- Gordon, B. L. et al. Why does snowmelt-driven streamflow response to warming vary? A data-driven review and predictive framework. *Environ. Res. Lett.* **17**, 053004 (2022).
- Hamlet, A. F. & Lettenmaier, D. P. Effects of 20th century warming and climate variability on flood risk in the western U. S. *Water Resour. Res.* **43**, 2006WR005099 (2007).
- Hirsch, R. M. & Archfield, S. A. Not higher but more often. *Nat. Clim. Change* **5**, 198–199 (2015).
- Musselman, K. N., Keitholotch, N. P., Mar, N. & Mgulis, S. A. Snowmelt response to simulated warming across a large elevation gradient, southern sierra Nevada, California. *Cryosphere* **11**, 2847–2866 (2017).
- Klos, P. Z., Link, T. E. & Abatzoglou, J. T. Extent of the rain-snow transition zone in the western US under historic and projected climate. *Geophys. Res. Lett.* **41**, 4560–4568 (2014).
- Knowles, N., Dettinger, M. D. & Cayan, D. R. Trends in snowfall versus rainfall in the western United States. *J. Clim.* **19**, 4545–4559 (2006).
- Han, J. et al. Streamflow seasonality in a snow-dwindling world. *Nature* **629**, 1075–1081 (2024).
- Clow, D. W. Changes in the timing of snowmelt and streamflow in Colorado: a response to recent warming. *J. Clim.* **23**, 2293–2306 (2010).
- Field, C. B. *Managing the risks of extreme events and disasters to advance climate change adaptation: special report of the Intergovernmental Panel on Climate Change*. (Cambridge University Press, 2012).
- Yang, D. Siberian Lena River hydrologic regime and recent change. *J. Geophys. Res. Atmos.* **107**, ACL 14-1–ACL 14-10 (2002).
- Regonda, S. K., Rajagopalan, B., Clark, M. & Pitlick, J. Seasonal cycle shifts in hydroclimatology over the western United States. *J. Clim.* **18**, 372–384 (2005).
- Cunderlik, J. M. & Ouara, T. B. M. J. Trends in the timing and magnitude of floods in Canada. *J. Hydrol.* **375**, 471–480 (2009).
- Ryberg, K. R., Akyue, F. A., Wiche, G. J. & Lin, W. Changes in seasonality and timing of peak streamflow in snow and semi-arid climates of the north-central United States, 1910–2012. *Hydrol. Process.* **30**, 1208–1218 (2016).
- Burn, D. H. & Whitfield, P. H. Changes in flood events inferred from centennial length streamflow data records. *Adv. Water Resour.* **121**, 333–349 (2018).
- Blöschl, G. et al. Changing climate shifts timing of European floods. *Science* **357**, 588–590 (2017).
- Vormoor, K., Lawrence, D., Schlichting, L., Wilson, D. & Wong, W. K. Evidence for changes in the magnitude and frequency of observed rainfall vs. snowmelt driven floods in Norway. *J. Hydrol.* **538**, 33–48 (2016).
- Hodgkins, G. A. & Dudley, R. W. Changes in the timing of winter-spring streamflows in eastern North America, 1913–2002. *Geophys. Res. Lett.* **33**, 2005GL025593 (2006).
- Musselman, K. N. et al. Projected increases and shifts in rain-on-snow flood risk over western North America. *Nat. Clim. Change* **8**, 808–812 (2018).
- Stein, L., Pianosi, F. & Woods, R. Event-based classification for global study of river flood generating processes. *Hydrol. Process.* **34**, 1514–1529 (2020).
- Milly, P. C. D. & Dunne, K. A. Colorado River flow dwindles as warming-driven loss of reflective snow energizes evaporation. *Science* **367**, 1252–1255 (2020).
- Godsey, S. E., Kirchner, J. W. & Tague, C. L. Effects of changes in winter snowpacks on summer low flows: case studies in the Sierra Nevada, California, USA. *Hydrol. Process.* **28**, 5048–5064 (2014).
- Liu, Z., Wang, T., Han, J., Yang, W. & Yang, H. Decreases in mean annual streamflow and interannual streamflow variability across snow-affected catchments under a warming climate. *Geophys. Res. Lett.* **49**, e2021GL097442 (2022).
- Davenport, F. V., Herrera-Estrada, J. E., Burke, M. & Diffenbaugh, N. S. Flood size increases nonlinearly across the Western United States in response to lower snow-precipitation ratios. *Water Resour. Res.* **56**, e2019WR025571 (2020).
- Henn, B., Musselman, K. N., Lestak, L., Ralph, F. M. & Molotch, N. P. Extreme runoff generation from atmospheric River Driven Snowmelt during the 2017 Oroville Dam Spillways Incident. *Geophys. Res. Lett.* **47**, e2020GL088189 (2020).

33. Arnell, N. W. & Gosling, S. N. The impacts of climate change on river flood risk at the global scale. *Climatic Change* **134**, 387–401 (2016).
34. Cayan, D. R., Kammerdiener, S. A., Dettinger, M. D., Caprio, J. M. & Peterson, D. H. Changes in the onset of spring in the western United States. *Bull. Am. Meteorol. Soc.* **82**, 399–416 (2001).
35. Bintanja, R. & Andry, O. Towards a rain-dominated Arctic. *Nat. Clim. Change* **7**, 263–267 (2017).
36. Qin, Y. Agricultural risks from changing snowmelt. *Nat. Clim. Change* **10**, 459–465 (2020).
37. Musselman, K. N., Clark, M. P., Liu, C., Ikeda, K. & Rasmussen, R. Slower snowmelt in a warmer world. *Nat. Clim. Change* **7**, 214–219 (2017).
38. Wu, X., Che, T., Li, X., Wang, N. & Yang, X. Slower snowmelt in spring along with climate warming across the Northern Hemisphere. *Geophys. Res. Lett.* **45**, 12,331–312,339 (2018).
39. Barnhart, T. B. et al. Snowmelt rate dictates streamflow. *Geophys. Res. Lett.* **43**, 8006–8016 (2016).
40. Mu, C. The status and stability of permafrost carbon on the Tibetan Plateau. *Earth-Sci. Rev.* **211**, 103433 (2020).
41. Brunner, M. I. & Dougherty, E. M. Varying Importance of Storm Types and Antecedent Conditions for Local and Regional Floods. *Water Resour. Res.* **58**, e2022WR033249 (2022).
42. Poff, N. L. et al. The natural flow regime. *BioScience* **47**, 769–784 (1997).
43. Siebert, S. A global data set of the extent of irrigated land from 1900 to 2005. *Hydrol. Earth Syst. Sci.* **19**, 1521–1545 (2015).
44. Friedl, M. & Sulla-Menashe, D. (NASA EOSDIS Land Processes Distributed Active Archive Center, 2022).
45. Lehner, B. et al. High-resolution mapping of the world's reservoirs and dams for sustainable river-flow management. *Front. Ecol. Environ.* **9**, 494–502 (2011).
46. Muñoz-Sabater, J. et al. ERA5-Land: A state-of-the-art global reanalysis dataset for land applications. *Earth Syst. Sci. Data* **13**, 4349–4383 (2021).
47. Ombadi, M., Risser, M. D., Rhoades, A. M. & Varadharajan, C. A warming-induced reduction in snow fraction amplifies rainfall extremes. *Nature* **619**, 305–310 (2023).
48. Copernicus Climate Change Service, Climate Data Store. ERA5 post-processed daily-statistics on single levels from 1940 to present. Copernicus Climate Change Service (C3S) Climate Data Store (CDS). <https://doi.org/10.24381/cds.4991cf48> (2024).
49. Luo, J. et al. GlobSnow v3.0 northern hemisphere snow water equivalent dataset. *Sci. Data* **8**, 163 (2021).
50. Lang, M., Ouarda, T. B. M. J. & Bobée, B. Towards operational guidelines for over-threshold modeling. *J. Hydrol.* **225**, 103–117 (1999).
51. Xie, J. et al. Evaluation of typical methods for baseflow separation in the contiguous United States. *J. Hydrol.* **583**, 124628 (2020).
52. Tarasova, L., Basso, S., Zink, M. & Merz, R. Exploring controls on rainfall-runoff events: 1. Time series-based event separation and temporal dynamics of event runoff response in Germany. *Water Resour. Res.* **54**, 7711–7732 (2018).
53. Tarasova, L. et al. Causative classification of river flood events. *Wiley Interdiscip. Rev. Water* **6**, e1353 (2019).
54. Duan, Q., Sorooshian, S. & Gupta, V. K. Optimal use of the SCE-UA global optimization method for calibrating watershed models. *J. Hydrol.* **158**, 265–284 (1994).
55. Fontrodona-Bach, A., Schaeffli, B., Woods, R., Teuling, A. J. & Larsen, J. R. N. H.-S. W. E. Northern Hemisphere Snow Water Equivalent dataset based on in situ snow depth time series. *Earth Syst. Sci. Data* **15**, 2577–2599 (2023).
56. Guo, Y. Warming leads to both earlier and later snowmelt floods over the past 70 years. idfloodPy. Zenodo <https://doi.org/10.5281/zenodo.15117546> (2025).

Acknowledgements

This study is financially supported by the Ministry of Science and Technology of China [Grant No. 2023YFC3006702 (Y.Y.), 2023YFC3206603 (Y.Y.), 2023YFC3206300 (Y.D.)] and the Department of Science and Technology of Qinghai Province [Grant No. 2024-SF-A6 (Y.Y.)].

Author contributions

Y.G., Y.Y., and D.Y. initiated the idea and designed the study. Y.G. and Y.Y. performed the analyses with help from J.X. and F.R., Y.G. and Y.Y. drafted the manuscript. L.Z., H.Z., J.H., Z.L. contributed to the results discussion and the review and editing of the manuscript. Y.Y. and Y.D. acquired funding for this research.

Competing interests

The authors declare no competing interests.

Additional information

Supplementary information The online version contains supplementary material available at <https://doi.org/10.1038/s41467-025-58832-0>.

Correspondence and requests for materials should be addressed to Yuting Yang or Dawen Yang.

Peer review information *Nature Communications* thanks the anonymous reviewers for their contribution to the peer review of this work. A peer review file is available.

Reprints and permissions information is available at <http://www.nature.com/reprints>

Publisher's note Springer Nature remains neutral with regard to jurisdictional claims in published maps and institutional affiliations.

Open Access This article is licensed under a Creative Commons Attribution-NonCommercial-NoDerivatives 4.0 International License, which permits any non-commercial use, sharing, distribution and reproduction in any medium or format, as long as you give appropriate credit to the original author(s) and the source, provide a link to the Creative Commons licence, and indicate if you modified the licensed material. You do not have permission under this licence to share adapted material derived from this article or parts of it. The images or other third party material in this article are included in the article's Creative Commons licence, unless indicated otherwise in a credit line to the material. If material is not included in the article's Creative Commons licence and your intended use is not permitted by statutory regulation or exceeds the permitted use, you will need to obtain permission directly from the copyright holder. To view a copy of this licence, visit <http://creativecommons.org/licenses/by-nc-nd/4.0/>.

© The Author(s) 2025